eprints@whiterose.ac.uk
https://eprints.whiterose.ac.uk/

Torque Density Enhancement of 6/4 Variable Flux Reluctance Machine with 2nd Harmonic Current Injection

J.H. Feng, L.R. Huang, Z.Q. Zhu, Fellow, IEEE, S.Y. Guo and J.X. Shi

Abstract—Variable flux reluctance machines (VFRMs) are developed as magnetless electrical machines. To extend the application of VFRMs, the enhancement of torque density is a key during machine design. In this paper, a novel 2nd harmonic current injection method is developed for torque density enhancement for 6-stator-slot/4-rotor-tooth (6/4) VFRM. By using the analytical method, the optimal current profile with injected 2nd harmonic current is obtained. The average torque of 6/4 VFRM is improved by 20% with the proposed method under all load conditions. Moreover, the proposed current profile has fixed harmonic proportions and is easily applicable to machines with different specifications. All the conclusions are confirmed by both finite element analyses and experimental results.

Index Terms— Harmonic current injection method, reluctance machine, torque density.

I. INTRODUCTION

PERMANENT magnet (PM) machines have been widely used in domestic and industrial applications due to their excellent performance. However, with the increasing concerns about the cost, resource, and risk of demagnetization of PMs [1], many magnetless machines have been extensively investigated recently [2][3].

As one kind of magnetless machines, variable flux reluctance machines (VFRMs) are developed in [4]-[6]. Fig. 1 shows the structure and configuration of a 6-stator-slot/4-rotor-tooth (6/4) VFRM. It has an identical double-salient structure as a switched reluctance machine (SRM). However, two sets of concentrated windings, i.e., AC-excited armature winding and DC-excited field winding, are located in the stator. It is proved by the torque production mechanism analysis in [7][8] that VFRMs are actually one kind of stator-wound-field synchronous machines. In [9], the electromagnetic performance of VFRMs is comprehensively investigated. Compared with SRMs, the VFRMs are reported to have several advantages, e.g., lower acoustic noise and vibration, more flexible rotor pole number selection, feasible application of commercial three-phase inverter and no requirement of slip-ring/brush.

J.H. Feng, S.Y. Guo, and J.X. Shi are with the CRRC Zhuzhou Institute Co. Ltd, Shidai Road, Shifeng District, Zhuzhou, Hunan, China (e-mail: fengjh@csrzic.com; guosy@csrzic.com; shijx2@csrzic.com;)

L.R. Huang and Z.Q. Zhu are with the Electrical Machines and Drives Group, University of Sheffield, Sheffield S1 3JD, U.K. (e-mail: lhuang18@sheffield.ac.uk; z.q.zhu@sheffield. ac.uk).
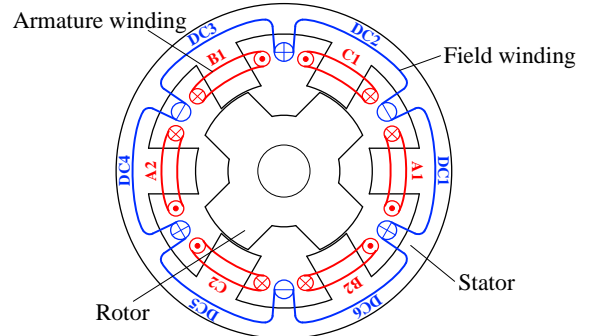

Fig. 1. Structure and winding configuration of 6/4 VFRM.

However, as a magnetless machine, the relatively low torque density of VFRM is a barrier that constraints its application. Several attempts related to the machine optimization are reported to successfully improve the output torque of VFRMs by properly selecting the structural parameters [10][11]. However, the torque density of VFRMs is still limited by the thermal constraint. In [12] and [13], an open-winding and a duel-three phase control methods are proposed to successfully reduce the copper loss of VFRMs by integrating the DC and AC windings. In this case, the torque density of VFRMs can be improved by using larger electric loading under the same thermal constraint. However, the cost of the inverter is also increased with these control methods. In this paper, a 2nd harmonic current injection method is developed to improve the torque density of 6/4 VFRM.

In fact, the harmonic current injection method is a technique that is frequently used to suppress the torque ripple of all kinds of electrical machines, e.g., brushless DC motor [14], flux-switching PM motor [15], interior PM synchronous motor [16] and VFRM [17]. It is also reported to be used for torque density enhancement for multi-phase PM and induction machines [18]-[21]. However, the harmonic current injection is seldom used to enhance the torque density of three-phase electric machines. In this paper, the AC current profile of 6/4 VFRM is optimized by injecting additional 2nd harmonic current. With this method, the torque density of VFRM can be improved by 20% at a fixed total RMS current.

The paper is organized as follows: Firstly, the torque mechanism of VFRM is briefly introduced in Section II. Based on this, the potential torque production of the 2nd harmonic current injection is investigated in Section III. Further, in Section IV, the 2nd harmonic current injection method is

developed by optimizing the amplitudes and initial phases of all the current components with an analytical model. Then, the electromagnetic performance of the proposed method is evaluated by finite element analysis (FEA) in Section V. In Section VI, the influence of 2nd harmonic current injection method on optimal machine dimension is analyzed. Finally, the experimental results of a 6/4 VFRM prototype is presented to validate all the investigations.

II. TORQUE PRODUCTION MECHANISM OF VFRMs

According to [7], the torque production of 6/4 VFRM can be explained by the magnetic gearing effect, as shown in Fig. 2. Basically, two magneto-motive-force (MMFs), i.e., MMF I and MMF II, are generated by excitations on stator (the two MMFs could originate from either two excitations or one excitation alone). They are then modulated by the salient rotor permeance, resulting in two magnetic fields, i.e., field I and field II. Both of these two fields consist of many harmonics. Taking the interaction between one specific component of field I and one specific component of field II for example, it is proved that:

(a) If these two field components have different pole pair numbers, the interaction between them has no contribution to the torque production.

(b) If these two field components only have identical pole pair numbers but different rotating speeds, they will only result in torque ripple. The frequency of torque ripple is determined by the rotating speed difference between two field components.

(c) If these two field components have identical pole pair numbers and rotating speeds, the interaction between them will contribute to average torque. The magnitude of average torque is determined by the amplitudes of two field components and the phase shift between them.

In this case, once the pole pair numbers of MMFs and rotor pole number are properly selected, there will be average torque generated. This is the general operation principle of VFRMs. From another perspective, the MMFs are equivalent to the outer and inner magnets of the magnetic gear, whereas the salient rotor permeance acts the role as the iron modulators of the magnetic gear. This is the "magnetic gearing effect" in VFRMs.
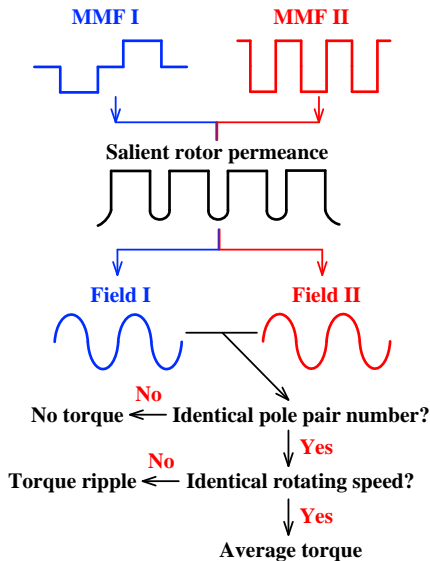

Fig. 2. Operation principle of VFRMs.

Based on this theory, the principles of average torque and torque ripple productions can be identified by airgap field harmonic analysis [7]. Firstly, assuming the general expression of two interactive MMFs and rotor permeance are:

$$\begin{cases} F_1(\theta,t) = \sum_{m=1}^{\infty} f_m \cos\left(P_m\theta - \Omega_m t - \theta_m\right) \\ F_2(\theta,t) = \sum_{n=1}^{\infty} f_n \cos\left(P_n\theta - \Omega_n t - \theta_n\right) \end{cases} \quad (1)$$

$$\Lambda_r(\theta,t) = \Lambda_{r0} + \sum_{k=1}^{\infty} \Lambda_{rk} \cos\left[kN_r\left(\theta - \Omega_r t - \theta_{r0}\right)\right] \quad (2)$$

where (f_m, f_n) (Ω_m, Ω_n) and (θ_m, θ_n) are the magnitudes, rotating speeds and initial phase of the (P_m, P_n)-th harmonics for MMF I and MMF II, respectively. N_r is the number of rotor teeth; Λ_{r0} and Λ_{rk} are the magnitudes of the dc and the kN_r-th rotor permeance harmonics, respectively; Ω_r is the rotor mechanical rotating speed; and θ_{r0} is the rotor initial position.

Then, for a specific combination of P_m-th component of MMF I, P_n-th component of MMF II, and kN_r-th component of rotor permeance, the interaction between them can lead to average torque only when conditions (3) and (4) are satisfied simultaneously.

$$kN_r = |P_m \pm P_n| \quad (3)$$

$$kN_r\Omega_r = \text{sgn}\left(P_m \pm P_n\right)\left(\Omega_m \pm \Omega_n\right) \quad (4)$$

The magnitude of average torque is governed by:

$$T_{avg}\left(kN_r, P_m, P_n\right) \propto kN_r \Lambda_{rk} f_m f_n \quad (5)$$

However, if only condition (3) is satisfied, the torque ripple rather than the average torque will be resulted. The times of fluctuation over one electrical period N_{ripple} is:

$$N_{ripple} = \left| k - \frac{\text{sgn}\left(P_m \pm P_n\right)\left(\Omega_m \pm \Omega_n\right)}{N_r\Omega_r} \right| \quad (6)$$

Since condition (3) is essential for both average torque and torque ripple productions, a specific combination of P_m-th component of MMF I, P_n-th component of MMF II, and kN_r-th component of rotor permeance, which satisfies (3) is defined as a "magnetic gear pair" in the following investigation.

III. TORQUE PRODUCTION OF 2ND HARMONIC CURRENT

Based on the theory introduced in Section II, the torque production of VFRMs with arbitrary excitation can be estimated. In this section, the potential torque production of the 2nd harmonic current is investigated for 6/4 VFRM.

A. Harmonic Contents of MMFs and Rotor Permeance in 6/4 VFRM

In a conventional VFRM, the field winding is excited by DC current I_f, whereas the armature winding is excited by a set of sinusoidal current (I_a, I_b, I_c). Their general expressions are:

$$I_f = I_0 \quad (7)$$

$$\begin{cases} I_a(t) = I_1 \sin\left(\omega_e t + \alpha_0\right) \\ I_b(t) = I_1 \sin\left(\omega_e t - 2\pi/3 + \alpha_0\right) \\ I_c(t) = I_1 \sin\left(\omega_e t + 2\pi/3 + \alpha_0\right) \end{cases} \quad (8)$$

where I_0 and I_1 are the amplitudes of DC and fundamental AC current component, respectively. ω_e is the electrical rotating speed, α_0 is the current advanced angle.

The torque enhancement method developed in this paper is to inject the 2nd harmonic current into the armature winding. Hence, the AC excitation can be expressed as:

$$\begin{cases} I_a(t) = I_1 \sin(\omega_e t + \alpha_0) + I_2 \sin(2\omega_e t + \beta_0) \\ I_b(t) = I_1 \sin(\omega_e t - 2\pi/3 + \alpha_0) + I_2 \sin(2\omega_e t + 2\pi/3 + \beta_0) \\ I_c(t) = I_1 \sin(\omega_e t + 2\pi/3 + \alpha_0) + I_2 \sin(2\omega_e t - 2\pi/3 + \beta_0) \end{cases} \quad (9)$$

According to the winding configuration of 6/4 VFRM in Fig. 1, its field winding is configured into 3-pole-pairs, whereas the armature winding is configured into 1-pole-pair. Therefore, the spatial harmonic content of MMFs generated by DC, 1st and 2nd currents can be deduced from the conventional winding theory, as shown in Table I. Meanwhile, the spatial harmonic content of rotor permeance is shown in Table II.

Further, by using Tables I and II and conditions (3)-(6), the torque production of VFRMs with and without the 2nd harmonic current injection can be estimated.

TABLE I
SPATIAL HARMONIC CONTENTS OF MMFs GENERATED BY DC, 1ST AND 2ND CURRENT COMPONENTS

Currents	Harmonic order	Specific harmonic	Rotating speed
I_0	6i+3	3, 9, 15…	0
I_1	6i+1	1, 7, 13…	$N_r\Omega_r$
	6i+5	5, 11, 17…	$-N_r\Omega_r$
I_2	6i+1	1, 7, 13…	$-2N_r\Omega_r$
	6i+5	5, 11, 17…	$2N_r\Omega_r$

TABLE II
SPATIAL HARMONIC CONTENTS OF ROTOR PERMEANCE

Λ_r	Harmonic order	Specific harmonic	Rotating speed
Λ_{rk}	4k	4, 8, 12…	$kN_r\Omega_r$

B. 6/4 VFRM without 2nd Harmonic Current Injection

In a 6/4 VFRM without the 2nd harmonic current injection, its torque production could be from the interactions between DC&DC, 1st&1st and DC&1st. They are actually the cogging torque, reluctance torque and synchronous torque according to the definition of a regular synchronous machine. The dominant magnetic gear pairs of average torque and torque ripple in a conventional 6/4 VFRM is shown in Tables III and IV, respectively. Some features can be revealed:

(a) The average torque is mainly from the interaction between DC and 1st currents (synchronous torque), whereas the other two torque components are negligible in terms of average value.

(b) The torque ripple is mainly from the interaction of 1st current itself (reluctance torque).

C. 6/4 VFRM with 2nd Harmonic Current Injection

When the additional 2nd harmonic current is injected into armature winding, the torque production of 6/4 VFRM can be divided into 6 components, i.e., DC&DC, 1st&1st, 2nd&2nd, DC&1st, DC&2nd and 1st&2nd. The dominant magnetic gear pairs of all the torque components are listed in Tables V and VI.

Some features can be revealed:

(a) The DC&1st and 1st&2nd components are dominant in average torque, whereas the other torque components are negligible in terms of average value.

(b) The torque ripple is mainly from the 1st&1st, 2nd&2nd and

DC&2nd components.

Overall, compared with the conventional 6/4 VFRM, the injected 2nd harmonic current is able to produce additional average torque from the interaction between the 1st and 2nd currents, and additional torque ripple from the interactions of 2nd&2nd and DC&2nd currents.

TABLE III
MAGNETIC GEAR PAIRS OF AVERAGE TORQUE FOR 6/4 VFRM WITHOUT 2ND HARMONIC CURRENT

Average torque	Permeance Λ_{rk}	kN_r	Source-harmonic P_m	P_n
DC&DC	-	-	-	-
1st&1st	Λ_{r2}	8	I_1 -1	I_1 -7
DC&1st	Λ_{r1}	4	I_0 -3	I_1 -1
			I_0 -3	I_1 -7

-Dominant components

TABLE IV
MAGNETIC GEAR PAIRS OF TORQUE RIPPLE FOR 6/4 VFRM WITHOUT 2ND HARMONIC CURRENT

Torque ripple	Permeance Λ_{rk}	kN_r	Source-harmonics P_m	P_n	N_{ripple}
DC&DC	Λ_{r3}	12	I_0 -3	I_0 -9	3
1st&1st	Λ_{r1}	4	I_1 -1	I_1 -5	3
DC&1st	Λ_{r2}	8	I_0 -3	I_1 -5	3

-Dominant components

TABLE V
MAGNETIC GEAR PAIRS OF AVERAGE TORQUE FOR 6/4 VFRM WITH 2ND HARMONIC CURRENT

Average torque	Permeance Λ_{rk}	kN_r	Source-harmonic P_m	P_n
DC&DC	-	-	-	-
1st&1st	Λ_{r2}	8	I_1 -1	I_1 -7
2nd&2nd	Λ_{r4}	16	I_2 -5	I_2 -11
DC&1st	Λ_{r1}	4	I_0 -3	I_1 -1
			I_0 -3	I_1 -7
DC&2nd	Λ_{r2}	8	I_0 -3	I_2 -5
1st&2nd	Λ_{r1}	4	I_1 -1	I_2 -5
			I_1 -5	I_2 -1

-Dominant components

TABLE VI
MAGNETIC GEAR PAIRS OF TORQUE RIPPLE FOR 6/4 VFRM WITH 2ND HARMONIC CURRENT

Torque ripple	Permeance Λ_{rk}	kN_r	Source-harmonics P_m	P_n	N_{ripple}
DC&DC	Λ_{r3}	12	I_0 -3	I_0 -9	3
1st&1st	Λ_{r1}	4	I_1 -1	I_1 -5	3
2nd&2nd	Λ_{r1}	4	I_2 -1	I_2 -5	3
DC&1st	Λ_{r2}	8	I_0 -3	I_1 -5	3
DC&2nd	Λ_{r1}	4	I_0 -3	I_2 -1	3
			I_0 -3	I_2 -7	
1st&2nd	Λ_{r2}	8	I_1 -1	I_2 -7	3
			I_1 -7	I_2 -1	

-Dominant components

D. FEA Verification

In order to verify the torque features estimated from the magnetic gearing effect, a 6/4 VFRM with the 2nd harmonic current injection is analyzed by FEA. Its main specifications are listed in Table VII. The amplitudes of DC, 1st and 2nd harmonic currents are all set to 1A ($I_0=I_1=I_2=1A$). Meanwhile, in order to easily separate the torque component and verify the aforementioned conclusions, linear cores are employed (their

permeability is set to infinite). The influence of saturation will only change the amplitude of permeance rather than the spatial harmonic content of permeance. Hence, the conclusions verified under linear case will also be valid in the nonlinear scenario.

Fig. 3 shows the torque waveforms and Fig. 4 compares the contributions of all the torque components on the average torque and the torque ripple. Just as expected, N_{ripple} is 3 for all the components. Meanwhile, the average torque is mainly contributed by the DC&1st and 1st&2nd components, whereas the torque ripple is mainly contributed by the 1st&1st, 2nd&2nd and DC&2nd components.

TABLE VII
MAIN SPECIFICATIONS OF 6/4 VFRM

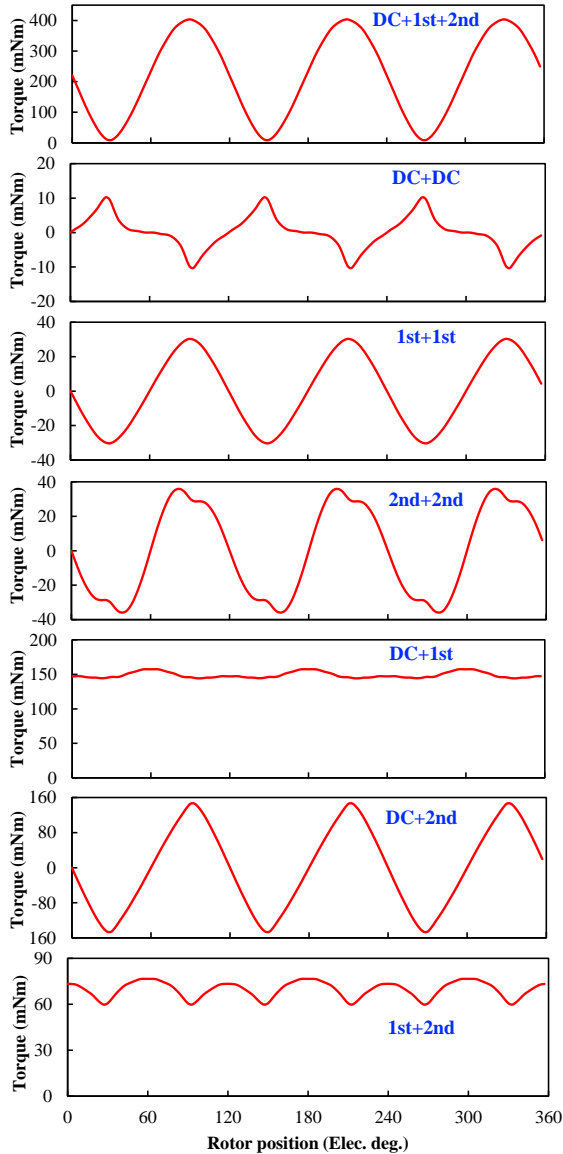| Parameter	Value	Parameter	Value
Airgap length	0.5 mm	Stator outer diameter	90 mm
Stator pole arc	30 deg.	Rotor outer diameter	46.4 mm
Rotor pole arc	41 deg.	Rated copper loss	30 W
Stack length	25 mm	Turns per coil (AC/DC)	183/183

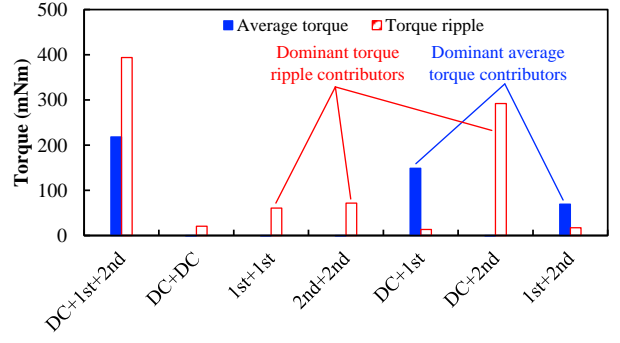Fig. 3. Waveforms of all the torque components for 6/4 VFRM. ($I_0=I_1=I_2=1$A, α_0=0deg., β_0=-90deg.)

Fig. 4. Contributions of all the components on average torque and torque ripple. ($I_0=I_1=I_2=1$A, α_0=0deg., β_0=-90deg.)

IV. 2ND HARMONIC CURRENT INJECTION METHOD

In Section III, it is proved that the 2nd harmonic current can generate additional average torque by the interaction between 1st and 2nd currents. This section further finalizes the 2nd harmonic current injection method by addressing the optimal amplitude and initial phase of the injected currents.

In [22], it is proved that the average torque of SRMs can be calculated from its phase inductance and current regardless of the influence of saturation, i.e.

$$T_{avg} = \frac{1}{2\pi} \int_0^{2\pi} \left[\frac{N_r}{2} \left(I_a^2 \frac{dL_a}{d\theta} + I_b^2 \frac{dL_b}{d\theta} + I_c^2 \frac{dL_c}{d\theta} \right) \right] d\theta \quad (10)$$

where L_a, L_b and L_c are the inductances of phases A, B and C, respectively.

Since the VFRMs have an identical structure as SRMs, this equation can also be used to calculate the average torque of VFRMs. In fact, the VFRMs are actually SRMs with arbitrary excitation. The excitation with the 2nd harmonic current can then be written into:

$$\begin{cases} I_a(t) = I_0 + I_1 \sin(\omega_e t + \alpha_0) + I_2 \sin(2\omega_e t + \beta_0) \\ I_b(t) = I_0 + I_1 \sin(\omega_e t - 2\pi/3 + \alpha_0) + I_2 \sin(2\omega_e t + 2\pi/3 + \beta_0) \\ I_c(t) = I_0 + I_1 \sin(\omega_e t + 2\pi/3 + \alpha_0) + I_2 \sin(2\omega_e t - 2\pi/3 + \beta_0) \end{cases} \quad (11)$$

According to [9] and [22], the inductance of 6/4 VFRM contains negligible mutual inductance between phases. Therefore, the inductance of all the phases can be expressed as

$$\begin{cases} L_a = L_0 + \sum_{k=1}^{\infty} L_k \cos(k\theta + \gamma_k) \\ L_b = L_0 + \sum_{k=1}^{\infty} L_k \cos[k(\theta - 2\pi/3) + \gamma_k] \\ L_c = L_0 + \sum_{k=1}^{\infty} L_k \cos[k(\theta + 2\pi/3) + \gamma_k] \end{cases} \quad (12)$$

where L_0 and L_k are the magnitudes of DC and k-th components of phase self-inductance; γ_k is the initial phase of k-th component of phase self-inductance.

By substituting (11) and (12) into (10), the average torque equation is deduced by harmonic analysis:

$$T_{avg\_012} = \frac{3N_r}{2} L_1 I_0 I_1 \cos(\gamma_1 - \alpha_0) + \frac{3N_r}{4} L_1 I_1 I_2 \sin(\gamma_1 + \alpha_0 - \beta_0) \quad (13)$$

where T_{avg_012} is the average torque of 6/4 VFRM generated by DC+1st+2nd harmonic currents.

In (13), the maximum average torque is obtained only when:

$$\begin{cases} \gamma_1 - \alpha_0 = 0 \\ \gamma_1 + \alpha_0 - \beta_0 = \pi/2 \end{cases} \quad (14)$$

Assuming the initial rotor position is at the aligned position (the rotor tooth is aligned with the center line of phase A), γ_1 is then 0 deg. In this case, the optimal initial phase will be:

$$\begin{cases} \gamma_1 = \alpha_0 = 0 \\ \beta_0 = -\pi/2 \end{cases} \tag{15}$$

T_{avg_012} can then be rewritten into:

$$T_{avg\_012} = \frac{3N_r}{2}L_1 I_0 I_1 + \frac{3N_r}{4}L_1 I_1 I_2 \tag{16}$$

Further, to reach the largest average torque/RMS current ratio, the total RMS current of VFRM is fixed to I_{rms}, i.e.

$$I_0^2 + I_1^2/2 + I_2^2/2 = I_{rms}^2 \tag{17}$$

To calculate the maximal value of T_{avg_012} under the condition of (17), the Lagrange multiplier method is applied, i.e.,

$$F(I_0, I_1, I_2, \lambda) = \frac{3N_r}{2}L_1 I_0 I_1 + \frac{3N_r}{4}L_1 I_1 I_2 + \lambda\left(I_0^2 + \frac{I_1^2}{2} + \frac{I_2^2}{2} - I_{rms}^2\right) \tag{18}$$

where λ is the Lagrange multiplier coefficient.

The maximal value of T_{avg_012} is obtained when I_0, I_1 and I_2 satisfy equation (19).

$$\begin{cases} \dfrac{dF}{dI_0} = \dfrac{3N_r}{2}L_1 I_1 + 2\lambda I_0 = 0 \\ \dfrac{dF}{dI_1} = \dfrac{3N_r}{2}L_1 I_0 + \dfrac{3N_r}{4}L_1 I_2 + \lambda I_1 = 0 \\ \dfrac{dF}{dI_2} = \dfrac{3N_r}{4}L_1 I_1 + \lambda I_2 = 0 \\ \dfrac{dF}{d\lambda} = I_0^2 + \dfrac{I_1^2}{2} + \dfrac{I_2^2}{2} - I_{rms}^2 = 0 \end{cases} \Rightarrow \sqrt{3}I_0 = I_1 = \sqrt{3}I_2 = I_{rms} \tag{19}$$

Therefore, the optimal excitation for the 2nd harmonic current injection method is:

$$\begin{cases} I_a(t) = \dfrac{I_{rms}}{\sqrt{3}} + I_{rms}\sin(\omega_e t) + \dfrac{I_{rms}}{\sqrt{3}}\sin\left(2\omega_e t - \dfrac{\pi}{2}\right) \\ I_b(t) = \dfrac{I_{rms}}{\sqrt{3}} + I_{rms}\sin\left(\omega_e t - \dfrac{2\pi}{3}\right) + \dfrac{I_{rms}}{\sqrt{3}}\sin\left(2\omega_e t + \dfrac{2\pi}{3} - \dfrac{\pi}{2}\right) \\ I_c(t) = \dfrac{I_{rms}}{\sqrt{3}} + I_{rms}\sin\left(\omega_e t + \dfrac{2\pi}{3}\right) + \dfrac{I_{rms}}{\sqrt{3}}\sin\left(2\omega_e t - \dfrac{2\pi}{3} - \dfrac{\pi}{2}\right) \end{cases} \tag{20}$$

The maximum average torque at a fixed RMS current I_{rms} is:

$$\max(T_{avg\_012}) = \frac{9N_r L_1 I_{rms}^2}{4\sqrt{3}} \tag{21}$$

The same method can also be applied to 6/4 VFRM without the 2nd harmonic current injection method. Its average torque expression, optimal proportion between I_0 and I_1, optimal excitation and maximum average torque are given by (22)-(25), respectively. The detailed derivation procedure is neglected here for simplicity.

$$T_{avg\_01} = \frac{3N_r}{2}L_1 I_0 I_1 \cos(\gamma_1 - \alpha_0) \tag{22}$$

$$\sqrt{2}I_0 = I_1 = I_{rms} \tag{23}$$

$$\begin{cases} I_a(t) = \dfrac{I_{rms}}{\sqrt{2}} + I_{rms}\sin(\omega_e t) \\ I_b(t) = \dfrac{I_{rms}}{\sqrt{2}} + I_{rms}\sin\left(\omega_e t - \dfrac{2\pi}{3}\right) \\ I_c(t) = \dfrac{I_{rms}}{\sqrt{2}} + I_{rms}\sin\left(\omega_e t + \dfrac{2\pi}{3}\right) \end{cases} \tag{24}$$

$$\max(T_{avg\_01}) = \frac{3N_r L_1 I_{rms}^2}{2\sqrt{2}} \tag{25}$$

where T_{avg_01} is the average torque of conventional 6/4 VFRM generated by DC and 1st harmonic currents.

(26) further compares the maximal average torques of 6/4 VFRM with and without 2nd harmonic current injection method. It can be seen that the developed 2nd harmonic current injection method is able to improve the average torque by 22% for 6/4 VFRM at a given total RMS current.

$$\frac{\max(T_{avg\_012})}{\max(T_{avg\_01})} = \frac{\sqrt{6}}{2} \approx 1.22 \tag{26}$$

V. ELECTROMAGNETIC PERFORMANCE EVALUATION OF 2ND HARMONIC INJECTION METHOD

To verify the electromagnetic performance of the proposed 2nd harmonic current injection method, the FEA results of a 6/4 VFRM with and without developed method are evaluated in this section. The main specifications are listed in Table VII. In order to account for the saturation effect, the core material is set to nonlinear.

A. Current Profiles

According to (20) and (23), the optimal current profiles of 6/4 VFRM with and without the 2nd harmonic injection method are compared in Fig. 5. It can be seen that, compared with the original pure sinusoidal AC current, the peak and peak-to-peak values of AC current with the 2nd harmonic current are increased by 58% and 18.6%, respectively. In contrast, the DC current is decreased by 18.4% with the developed method. Finally, the total RMS values of these two sets of current profiles are the same.
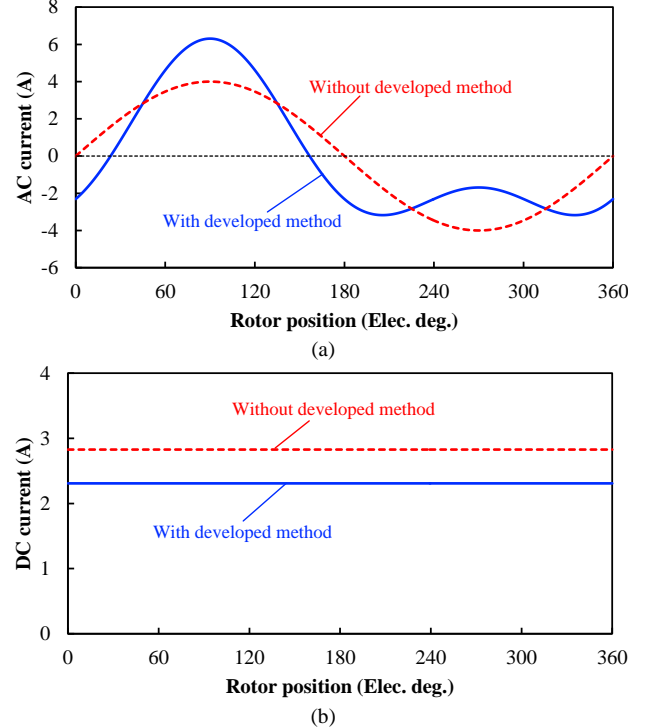
Fig. 5. Current profiles for VFRMs with and without 2nd harmonic injection method. ($I_{rms} = 4A$) (a) AC currents in armature winding. (b) DC currents in field winding.

B. Average Torque

In Section IV, it is predicted that the average torque of 6/4 VFRM can be enhanced by 22% with the developed 2nd harmonic current injection method. Since the average torque equations are valid under both unsaturated and saturated conditions, this conclusion is also valid for all the load conditions. Fig. 6 shows the variations of average torque with RMS current. It can be seen that a constant increase of 20% is achieved for average torque when the 2nd harmonic current injection method is used, confirming the effectiveness of the developed method.
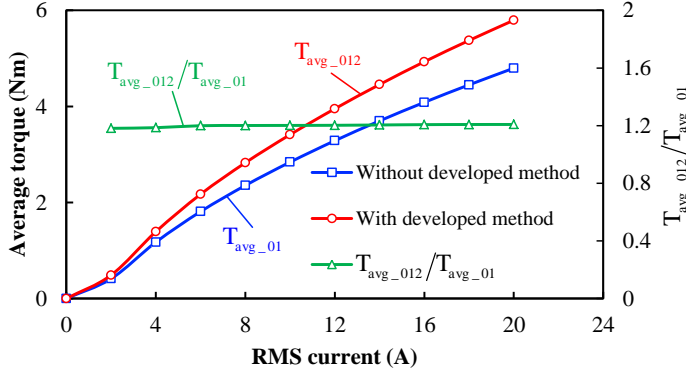

Fig. 6. Variations of average torque against total RMS current of VFRMs with and without 2nd harmonic current injection method.

C. Torque Ripple

As mentioned in Section II, the 2nd harmonic current will generate additional torque ripple by the interactions of DC&2nd and 2nd&2nd currents. As a result, the torque ripple of VFRM is expected to be increased with the proposed method. The torque waveforms and variations of torque ripple with RMS current for 6/4 VFRM with and without developed method are shown in Fig. 7. The torque ripple is decreasing with the RMS current. In addition, the torque ripple of VFRM with the 2nd harmonic current is significantly larger than that of conventional VFRM, which is a drawback of the proposed method.

D. Core Loss

The core loss should be evaluated when harmonic current is injected. The switching frequency of the magnetic field generated by the 2nd harmonic current is higher than that of the 1st harmonic current, which will lead to additional hysteresis loss and eddy current loss in cores. For evaluation, the core loss of VFRM with and without the 2nd harmonic injection is calculated by the ANSYS Maxwell 18.2 package. The iron loss model is:

$$P_{iron} = K_h f B_m^2 + K_c f^2 B_m^2 + K_e f^{1.5} B_m^{1.5} \qquad (27)$$

where P_{iron} is the core loss; K_h, K_c and K_e are the coefficients of hysteresis, eddy-current and excess losses; f is the frequency, B_m is the magnitude of flux density.

Fig. 8 compares the core losses of 6/4 VFRMs with and without the 2nd harmonic current injection. It can be seen that the core loss is increased by 17%~30% with the proposed method depending on the rotating speed. The higher the speed is, the higher the electrical frequency and the larger the increase in core loss will be.
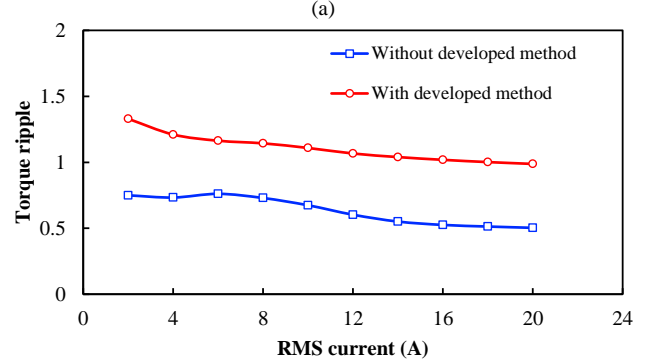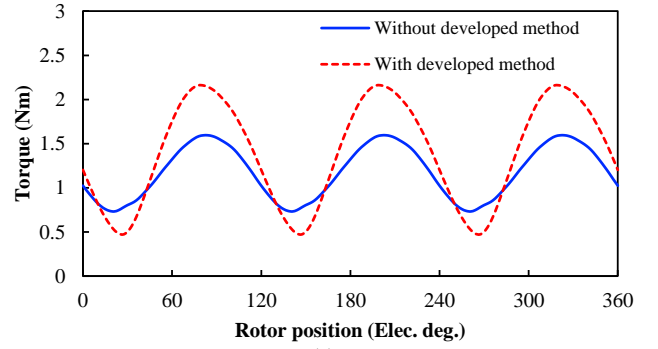

Fig. 7. Torque waveforms and variations of torque ripple with RMS current for VFRMs with and without 2nd harmonic current injection method. (a) Torque waveform ($I_{rms} = 4A$). (b) Torque ripple vs. RMS current.
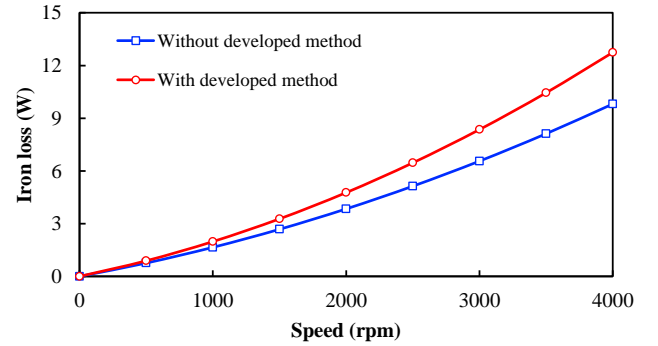

Fig. 8. Variations of core loss against rotating speed of VFRMs with and without 2nd harmonic current injection method. ($I_{rms} = 4A$).

E. Efficiency

The efficiency of VFRM is closely related to the core loss, copper loss and output power. It can be calculated by

$$\eta = \frac{P_{out}}{P_{out} + P_{cu} + P_{iron}} = \frac{T\Omega}{T\Omega + P_{cu} + P_{iron}} \times 100\% \qquad (28)$$

where η is the efficiency; P_{out}, P_{cu} and P_{iron} are the output power, copper loss and core loss; T is the output torque; Ω is the mechanical rotating speed.

When the performance of VFRM is evaluated under the same total RMS current, the variations of efficiency with rotating speed is shown in Fig. 9. It can be found that although the core loss is increased due to the injection of the 2nd harmonic current, the VFRM with developed method still shows higher efficiency than the conventional VFRM due to significant improvement in output power.
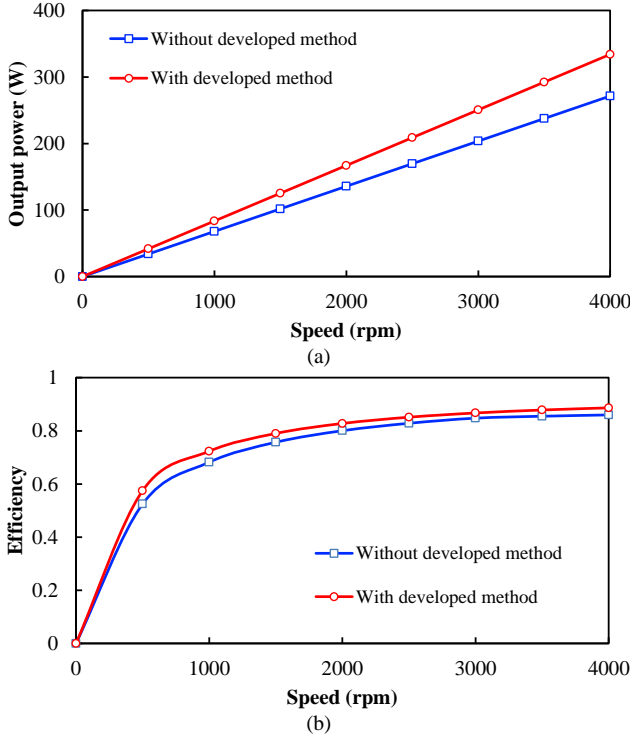
Fig. 9. Variations of output power and efficiency against rotating speed of VFRMs with and without 2-nd harmonic current injection method. (I_{rms} = 4A). (a) Power. (b) Efficiency.

VI. INFLUENCE OF 2ND HARMONIC CURRENT INJECTION ON OPTIMAL MACHINE DESIGN

From the foregoing investigation, it is proved that the proposed method is a modification of the current profile. This enables the method to be applied to the 6/4 VFRM with any specifications for an instant torque density enhancement. However, for a VFRM specifically designed with the 2nd harmonic current injection control scheme, the optimal machine dimensions will be different from those designed with a conventional current profile, which will be discussed in this section.

As can be seen from Fig. 5, the current profile with the 2nd harmonic current has a higher peak value than the conventional one, which eventually leads to more saturation in cores, as confirmed by the field distributions of 6/4 VFRM in Fig. 10.

Then, by using the constraints listed in Table VIII, the VFRM is globally optimized with the 2nd harmonic current injection method used. A comparison of the optimal dimensions of VFRM is presented in Table IX. It can be seen that, due to the severer saturation caused by the 2nd harmonic current, the split ratio and stator yoke thickness tend to increase whereas the rotor pole arc tends to decrease. This phenomenon agrees with the conclusions in [23] for VFRM design under difference copper loss. With a fixed copper loss condition, an increase in split ratio and stator yoke thickness will help suppress the electrical load and a decrease in rotor pole arc will reduce the flux linkage flowing from stator into rotor. Both aspects will alleviate the saturation in cores. Finally, with the optimized specification, a 22% increase in average torque is achieved with the developed method, albeit with a 171% increase in torque ripple as well.
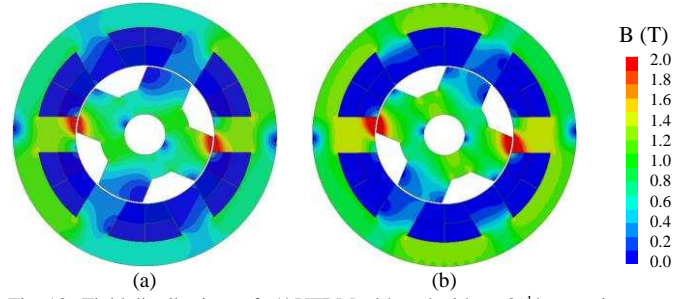

Fig. 10. Field distributions of 6/4 VFRM with and without 2nd harmonic current injection. (P_{cu}=30W). (a) Without 2nd harmonic. (b) With 2nd harmonic.

TABLE VIII
CONSTRAINTS OF GLOBAL OPTIMIZATION FOR VFRM WITH DEVELOPED METHOD

Parameter	Value	Parameter	Value
Airgap length	0.5 mm	Stator pole arc	25~35 deg.
Stack length	25 mm	Rotor pole arc	35~45 deg.
Stator outer diameter	90 mm	Split ratio	0.45~0.6
Turns per coil (AC/DC)	183/183	Stator yoke height	6~10 mm
Rated copper loss	30 W	Rotor yoke height	6~10 mm

TABLE IX
OPTIMAL DIMENSIONS OF VFRM WITH AND WITHOUT DEVELOPED METHOD

Parameter	Unit	Conventional	With 2nd harmonic current
Stator pole arc	deg.	30	30.5
Rotor pole arc	deg.	41	38
Split ratio	-	0.53	0.55
Stator yoke thickness	mm	7.8	8
Rotor yoke thickness	mm	8	8

TABLE X
COMPARISON OF TORQUE PERFORMANCE OF VFRM WITH AND WITHOUT DEVELOPED METHOD

	Without 2nd harmonic	With 2nd harmonic	
	Optimized	Before optimization	After optimization
Average torque (Nm)	0.77	0.92 (+19.5%)	0.94 (+22%)
Torque ripple (Nm)	0.45	1.14 (+153%)	1.22 (+171%)

VII. EXPERIMENTAL VERIFICATION

In order to verify the effectiveness of the proposed 2nd harmonic injection method, a 6/4 VFRM is prototyped and tested. The structure and main specification are shown in Fig. 11 and Table VII, respectively.
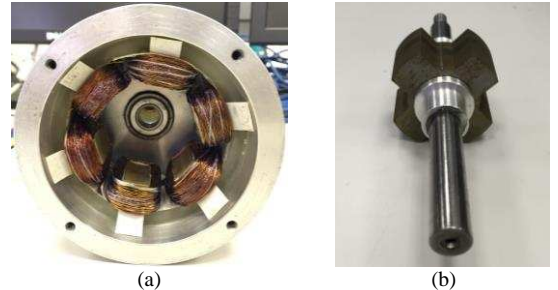

Fig. 11. Photos of 6s/4r VFRM prototype. (a) Stator. (b) Rotor.

It can be seen that each stator tooth is wound by two concentrated coils for armature and field winding. The control scheme of VFRM is presented in Fig. 12. The three-phase commercial inverter and space vector control method are applied to the armature winding, which are exactly the same as those of regular synchronous machine. For the field winding, an

external current control module is implemented to generate the DC current. The system is controlled by dSPACE control desk.
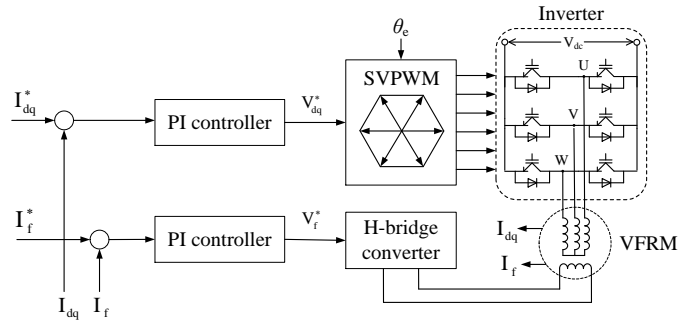

Fig. 12. Control scheme and drive circuit of 6/4 VFRM prototype.

Fig. 13 shows the test rig of the experiment. To measure the torque performance, the torque transducer is used. A brushed DC machine acts as a load on the test rig.
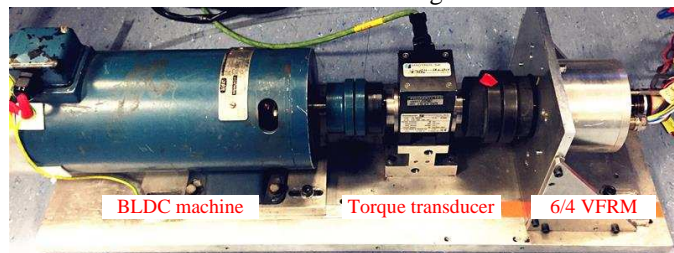

Fig. 13. Test rig.

Firstly, the back-EMF of the prototype is measured, as shown in Fig. 14. It can be seen that the measurements agree well with the FEA results. Moreover, although the waveforms of back-EMFs are trapezoidal, they contain negligible 2nd harmonic components. Therefore, there will be no average torque generated between the interaction of DC and 2nd harmonic currents, confirming the foregoing investigations.

Further, the performance of 6/4 VFRM with and without the 2nd harmonic injection is tested. Fig. 15 compares the measured rotating speed and current waveforms of VFRMs with and without the proposed method. Since there is only current control but no speed control in the drive system, the speed will fluctuate with the torque ripple. The larger the torque ripple is, the larger the fluctuation in speed will be. It can be clearly seen that the speed fluctuation of conventional VFRM without developed method is significantly smaller than that of VFRM with 2nd harmonic current injection. This indicates the larger torque ripple of the developed method. To further confirm this, the torque profiles of VFRMs with and without the 2nd harmonic injection are measured by torque transducer on the test rig shown in Fig. 13. During the test, the total RMS current is set to 1.5A. The DC, the 1st and 2nd current components are set accordingly based on (19) and (23). The torque measurement is conducted under a low speed (100rpm) to keep a stable current and avoid the influence of PWM as much as possible. The measured torque profiles have good agreement with the FEA predictions, albeit with some small fluctuations caused by the minor spikes in current, as can be found in Fig. 15.
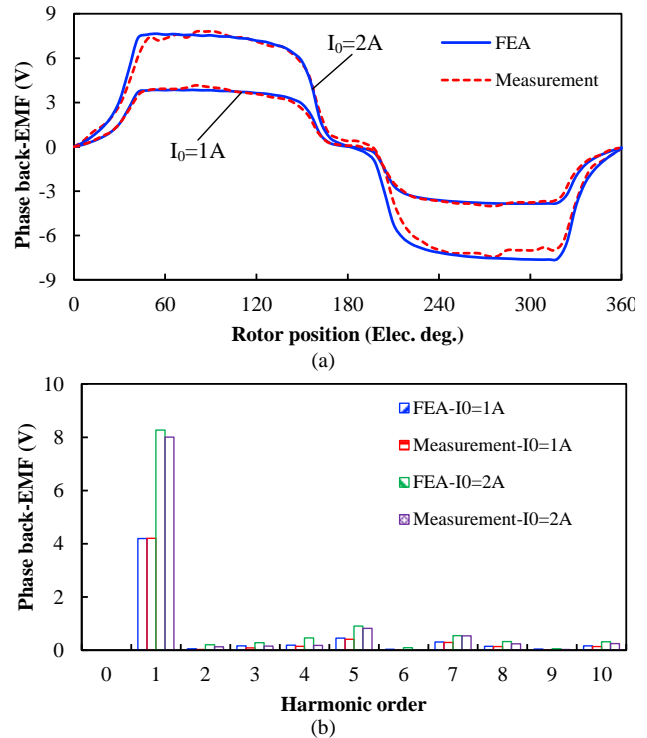

(a)

(b)

Fig. 14. Back-EMFs of 6/4 VFRM under 1A and 2A field currents and 400rpm. (a) Waveform. (b) Spectra.
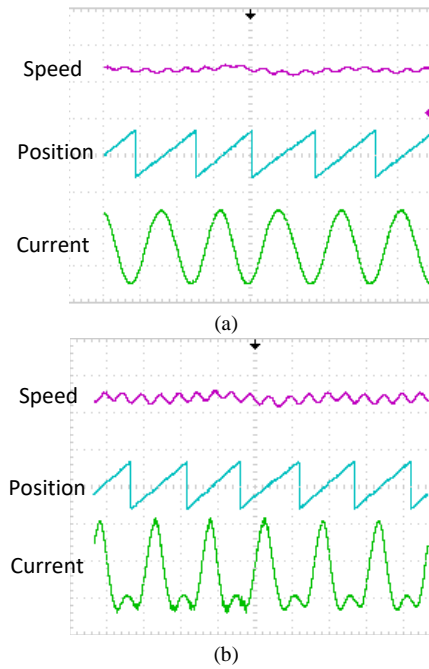

(a)

(b)

Fig. 15. Measured speed, position and AC current waveforms of 6/4 VFRM with and without developed method (I_{rms}=2A, 100rpm). (a) Without developed method. (b) With developed method.

Finally, the average torques of 6/4 VFRM with and without developed method are measured, as shown in Fig. 17. The average torque of VFRM with developed method is significantly larger than that of conventional VFRM, confirming the effectiveness of the proposed method.
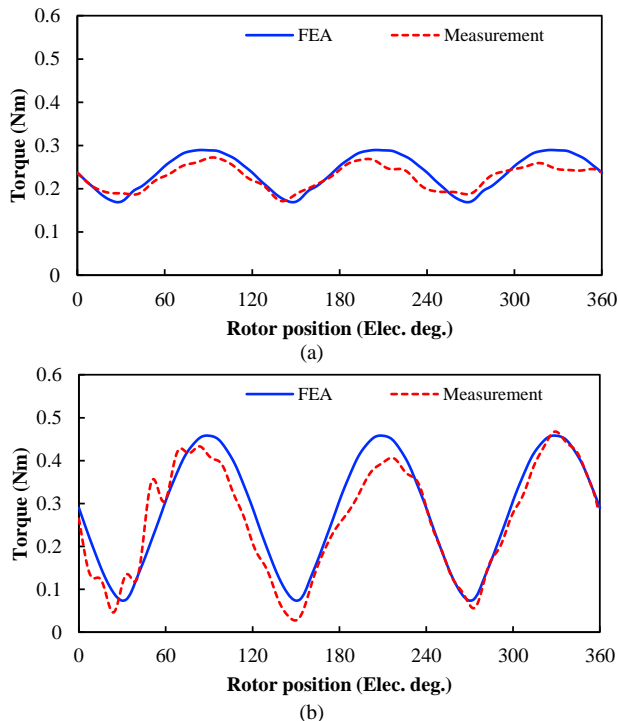
Fig. 16. Measured torque waveforms of 6/4 VFRM with and without developed method at 400rpm. (a) Without developed method (I_0=1.06A, I_1=1.5A). (b) With developed method (I_0=0.866A, I_1=1.5A, I_2=0.866A).
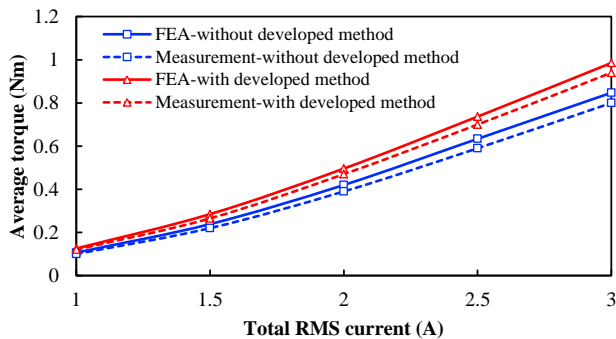

Fig. 17. Variations of average torque with total RMS current for 6/4 VFRM with and without developed method.

VIII. Conclusion

In this paper, a novel 2nd harmonic current injection method is proposed for torque density enhancement in a 6/4 VFRM. Firstly, based on the magnetic gearing effect, the 2nd harmonic current is found to be able to contribute to the average torque by the interaction of 1st&2nd currents, and the torque ripple by the interactions of DC&2nd and 2nd&2nd currents. Then, the optimal current profile of 6/4 VFRM with 2nd harmonic current injection is obtained based on an analytical model. The developed method is found to be able to increase the average torque by 20% under a fixed total RMS current. However, two evitable drawbacks, i.e., larger torque ripple and core loss, are also observed, which need to be improved in future work. The effectiveness of the proposed method is confirmed by both FEA and experimental results.

References

[1] I. Boldea, L. N. Tutelea, L. Parsa, and D. Dorrell, "Automotive electric propulsion systems with reduced or no permanent magnets: an overview," IEEE Trans. Ind. Electron., vol. 61, no. 10, pp. 5696-5711, Oct. 2014.

[2] C. Yu and S. Niu, "Development of a magnetless flux switching machine for rooftop wind power generation," IEEE Trans. Energy Convers., vol. 30, no. 4, pp. 1703-1711, Dec. 2015.

[3] C. H. T. Lee, K. T. Chau, and C. Liu, "Design and analysis of a cost-effective magnetless multiphase flux-reversal dc-field machine for wind power generation," IEEE Trans. Energy Convers., vol. 30, no.4, pp. 1565-1573, Dec. 2015.

[4] O. Ojo and Z. Wu, "Synchronous operation of a dual-winding reluctance generator," IEEE Trans. Energy Convers., vol. 12, no. 4, pp. 357-362, Dec. 1997.

[5] T. Fukami, Y. Matsuura, K. Shima, M. Momiyama, and M. Kawamura, "Development of a low-speed multi-pole synchronous machine with a field winding on the stator side," in Proc. Int. Conf. Elect. Mach., Rome, Italy, 2010, pp. 1–6.

[6] X. Liu, Z. Q. Zhu and Z. P. Pan, "Analysis of electromagnetic torque in sinusoidal excited switched reluctance machines having DC bias in excitation," in Proc. Int. Conf. Elect. Mach., Sept. 2012, pp. 2882-2888.

[7] L. R. Huang, J.H. Feng, S.Y. Guo, J.X. Shi, W.Q. Chu, and Z.Q. Zhu, "Analysis of torque production in variable flux reluctance machine," IEEE Trans. Energy Convers., vol. 32, no.4, pp. 1297-1308, Apr. 2017.

[8] S. Jia, R. Qu, J. Li, and D. Li, "Principles of stator DC winding excited Vernier reluctance machines," IEEE Trans. Energy Convers., vol. 31, no.3, pp. 935-946, Sept. 2016.

[9] X. Liu and Z. Q. Zhu, "Electromagnetic performance of novel variable flux reluctance machines with DC-field coil in stator," IEEE Trans. Magn., vol. 49, no. 6, pp. 3020-3028, Aug. 2012.

[10] J. T. Shi, X. Liu, D. Wu, and Z. Q. Zhu, "Influence of stator and rotor pole arcs on electromagnetic torque of variable flux reluctance machines," IEEE Trans. Magn., vol. 50, no. 11, pp. 1-4, Nov. 2014.

[11] J. Shaofeng, Q. Ronghai, and L. Jian, "Design considerations and parameter optimization of stator wound field synchronous machines based on magnetic the gear effect," in Proc. ECCE, Sept. 2015, pp. 5195-5202.

[12] Z. Q. Zhu, Beomseok Lee, Xu Liu, "Integrated field and armature current control strategy for variable flux reluctance machine using open winding," IEEE Trans. Ind. Appl., vol. 52, no. 2, pp. 1519–1529, Mar./Apr. 2016.

[13] Z. Q. Zhu, Beomseok Lee, "Integrated field and armature current control for dual three-phase variable flux reluctance machine drives," IEEE Trans. Energy Convers., vol. 32, no.2, pp. 447-457, Jun. 2017.

[14] H. Le-Huy, R. Perret, and R. Feuillet, "Minimization of torque ripple in brushless DC motor drives," IEEE Trans. Ind. Appl., vol. IA-22, no. 4, pp. 748–755, Jul./Aug. 1986.

[15] H. Jia, M. Cheng, W. Hua, W. Zhao, and W. Li, "Torque ripple suppression in flux-switching PM motor by harmonic current injection based on voltage space-vector modulation," IEEE Trans. Magn., vol. 46, no. 6, pp. 1527–1530, Jun. 2010.

[16] G. Lee, S. Kim, J. Hong, and J. Bahn, "Torque ripple reduction of interior permanent magnet synchronous motor using harmonic injected current," IEEE Trans. Magn., vol. 44, no. 6, pp. 1582–1585, Jun. 2008.

[17] Beomseok Lee, Z. Q. Zhu, L. R. Huang, "Torque ripple reduction for 6-stator/4-rotor-pole variable flux reluctance machines by using harmonic field current injection," IEEE Trans. Ind. Appl., vol. 53, no. 4, pp. 3730–3737, Jul./Aug. 2017.

[18] L. Parsa, H. A. Toliyat, "Five-phase permanent magnet motor drives," IEEE Trans. Ind. Appl., vol. 41, no. 1, pp. 30–37, Jan./Feb. 2005.

[19] K. Wang, Z. Gu, C. Liu, and Z. Q. Zhu, "Design and analysis of five phase SPM machine considering third harmonic current injection," IEEE Trans. Energy Convers., DOI: 10.1109/TEC.2018.2811399

[20] R. O. C. Lyra, T. A. Lipo, "Torque density improvement in a six-phase induction motor with third harmonic current injection," IEEE Trans. Ind. Appl., vol. 38, no. 5, pp. 1351-1360, Sep./Oct. 2002.

[21] A. S. Abdel-Khalik, S. Mostafa Gadoue, M. I. Masoud, and B. W. Wiliams, "Optimum flux distribution with harmonic injection for a multiphase induction machine using genetic algorithms," IEEE Trans. Energy Convers., vol. 26, no. 2, Jun. 2011.

[22] Z. Q. Zhu, Beomseok Lee, Liren Huang, Wenqiang Chu, "Contribution of current harmonics to average torque and torque ripple in switched reluctance machines," IEEE Trans. Magn., vol. 53, no. 3, pp. 1-4, Mar. 2017.

[23] L.R. Huang, J.H. Feng, S.Y. Guo, J.X. Shi, W.Q. Chu, and Z.Q. Zhu, "Fast design method of variable flux reluctance machines," CES Transactions on Electrical Machines and Systems, vol. 2, no.1, pp. 152-159, Mar. 2018.

J.H. Feng (S'06) received his B.S. and M.S. degrees in Electrical Machinery Control from Zhejiang University, China in 1986 and 1989, respectively, and Ph. D. degree in Control Theory and Control Engineering from Central South University, China in 2008. Since 1989, he has been with CRRC Zhuzhou Institute Co. Ltd., Zhuzhou, China, where he is presently the Vice President and Chief Technology Officer. He has published a number of journal and conference proceedings papers. His research interests are modeling, control, and communication of electrical systems, rail networks and high-speed trains. He is also a Guest Professor in Southwest Jiaotong University, Tongji University and Central South University.

L.R. Huang received the B.Eng. and M.Sc. degrees in electrical engineering from Zhejiang University, Hangzhou, China, in 2012 and 2015, respectively, and the Ph.D. degree in electrical and electronic engineering from The University of Sheffield, Sheffield, U.K., in 2018. Since 2018, he is working as research assistant in Sheffield Siemens Gamesa Renewable Energy Research Centre.

His major research interests include design and application of reluctance machines and permanent magnet machines.

Z.Q. Zhu (M'90–SM'00–F'09) received the B.Eng. and M.Sc. degrees in electrical and electronic engineering from Zhejiang University, Hangzhou, China, in 1982 and 1984, respectively, and the Ph.D. degree in electrical and electronic engineering from The University of Sheffield, Sheffield, U.K., in 1991.

Since 1988, he has been with The University of Sheffield, where he is currently a Professor with the Department of Electronic and Electrical Engineering, Head of the Electrical Machines and Drives Research Group, Royal Academy of Engineering/Siemens Research Chair, Academic Director of Sheffield Siemens Wind Power Research Centre, Director of Sheffield CRRC Electric Drives Technology Research Centre, Director of Midea Electrical Machines and Controls Centre. His current major research interests include the design and control of permanent-magnet brushless machines and drives for applications ranging from automotive through domestic appliances to renewable energy.

Prof. Zhu is a Fellow of Royal Academy of Engineering, UK.

S.Y. Guo is a professorial senior engineer. She got graduated from Central South University in December 1981, and serves as the chief technical expert in CRRC Zhuzhou Institute Co., Ltd. in the field of R&D of the electric machine systems for railway locomotive and electrical vehicle applications.

J.X. Shi received the B. Eng. and M. Sc. degrees in electrical engineering from South China University of Technology, Guangzhou, China in 2010 and 2013, respectively. Since 2013, he has been with CRRC Zhuzhou Institute Co., Ltd.

His major research interests include design and application of permanent magnet machines for electrical vehicle applications.